Full-field digital gradient sensing method for evaluating stress gradients in transparent solids

Chandru Periasamy and Hareesh V. Tippur*

Department of Mechanical Engineering, Auburn University, Alabama 36849, USA

*Corresponding author: tippuhv@auburn.edu

Received 11 October 2011; accepted 27 February 2012;
posted 6 March 2012 (Doc. ID 156216); published 18 April 2012

A full-field digital gradient sensing method is proposed for measuring small angular deflections of light rays due to local stresses in transparent planar solids. The working principle of the method is explained, and the governing equations are derived. The analysis shows that angular deflections of light rays can be linked to nonuniform changes in thickness and refractive index of the material. In mechanically loaded planar solids, the angular deflections can be further related to spatial gradients of first invariant of stresses under plane stress conditions. The proposed method is first demonstrated by capturing the angular deflection fields in two orthogonal directions for a thin plano-convex lens. The measured contours of constant angular deflection of light rays are in good agreement with the expected ones for a spherical wavefront. The method is also successfully implemented to study a stress concentration problem involving a line load acting on an edge of a large planar sheet. Again, the stress gradients, measured simultaneously along and perpendicular to the loading directions, are in good agreement with the analytical predictions. The measured stress gradients have also been used to estimate stresses in the load point vicinity where plane stress results hold. © 2012 Optical Society of America

OCIS codes: 100.2000, 120.3940, 280.4788.

1. Introduction

Full-field measurement of deformations, strains, and stresses is necessary for understanding failure mechanisms in solids and for quantifying the associated engineering parameters. Over the years, several optical methods–photoelasticity, moiré interferometry, laser speckle photography/interferometry, and coherent gradient sensing, to name a few–have served as measurement tools of experimental solid mechanics [1,2]. These methods generally demand special optical characteristics of the material being studied, sample surface preparation (birefringence, specular reflectivity, and grating deposition) and/or coherent optics to be implemented successfully. In recent years, however, aided by tremendous advances in digital photography, image processing techniques, and ubiquitous computational power, the digital image correlation (DIC) method has emerged as a popular optical metrology tool [3]. It requires little or no surface preparation, uses ordinary white light illumination, and can be fashioned to measure two-dimensional (2D) (planar) or three-dimensional (3D) displacement components. Further, DIC methods are capable of accurate measurement of displacements limited only by the experimental parameters such as pixel resolution of the camera, optical magnification, gray scale depth (texture and decoration) and image correlation algorithm employed. The measured strains from DIC, however, are of relatively lower accuracy due to a variety of reasons, including first order Taylor's series representation of displacement gradients or numerical differentiation of noisy displacement data. This could be an important issue near stress concentrations where steep stress

1559-128X/12/122088-10$15.00/0

gradients occur. In this context, it is attractive to have a method capable of directly measuring stress gradients in the whole field while preserving the simplicity and versatility offered by DIC.

Since mechanical designs for strength and safety are generally based on stresses, stress estimation using an optical method adds to its usefulness. A stress gradient measurement method offers advantage of obtaining stress fields via numerical integration (generally, numerical integration of a noisy data set is more robust when compared to numerical differentiation of the same) of measured data if boundary conditions are known. In many engineering problems, particularly those dealing with stress concentrations or singularities, far-field conditions typically involve vanishing/negligible stress gradients. Further, at locations far away from the stress riser, stresses can be evaluated relatively accurately by either using the boundary conditions of the problem or supplementing measurements with a numerical scheme (e.g., finite element analysis). This further motivates the current research to introduce a full-field optical method to first measure stress gradients and subsequently estimate stresses from those measurements.

In the current work, a stress gradient measurement method that is based on elasto-optic effect and uses a DIC approach is developed for mechanical characterization of optically transparent planar solids. It should be noted that the optical transparency requirement, although possibly appearing restrictive, is an essential characteristic of solids used in many engineering applications including automotive windshields, electronic displays, aircraft canopies, hurricane resistant windows, protective helmet visors, and transparent armor materials [4,5]. Over the years, there has also been a great deal of interest in developing novel transparent composites for a variety of other engineering applications [6–9], which could benefit from the proposed method.

A few previous works have taken advantage of optical transparency to study stresses and stress gradients in materials. A lateral shearing interferometer called coherent gradient sensing (CGS) has been developed to study static and dynamic fracture mechanics problems [10–13]. In these works, optical interference corresponding to stress gradients near stationary and growing cracks has been evaluated [14–16] and crack tip parameters extracted. A Mach–Zehnder interferometer to quantify stresses near an interfacial crack in optically transparent poly-methyl methacrylate (PMMA) has been reported [17]. A thickness change measurement method using electronic speckle pattern interferometry and based on a Michelson interferometer has been developed [18] for transparent plates. However, the method does not consider refractive index changes due to stresses.

In the following, a digital gradient sensing (DGS) method is proposed for optically transparent solids. The working principle of the method for detecting local angular deflections of light rays in transparent solids is explained and the governing equations are derived. Then, the method is calibrated by measuring angular deflections of light rays produced by a *thin* plano-convex lens. Subsequently, DGS is used to evaluate stress gradients near a line load acting along the straight edge of a large planar sheet that gives rise to stress concentration at the loading point. The measurements are directly compared with the analytical predictions for this problem. The measurements are also used to *estimate* stresses in the vicinity of the stress concentration. Finally, the results are summarized and conclusions are drawn.

2. Experimental Setup

The experimental setup for the DGS method is shown in Fig. 1. It consists of a uniformly illuminated speckle target, a planar transparent test object, and a digital camera. The target is a planar surface coated with a random speckle pattern produced by spraying it with fine mists of black and white paint. The transparent specimen to be tested is placed in front of and parallel to the target plane at a known distance Δ, where $\Delta =$ the distance between the mid-plane of the specimen and the target plane.

A camera fitted with a relatively long focal length lens is placed behind the specimen at a large distance $L(\gg \Delta)$ and focused on the target plane through the specimen in the region of interest. The target is uniformly illuminated using two white light sources. The illumination sources are situated sufficiently far away from the specimen to minimize thermal currents that may distort the speckle images and/or heat the specimen during the experiment. The digital camera settings and lens parameters are selected such that the aperture is sufficiently small for achieving a good focus of speckles on the target while keeping the salient features of the specimen plane (e.g., specimen edges, and load point) discernible in the recorded image for easy postprocessing of images.

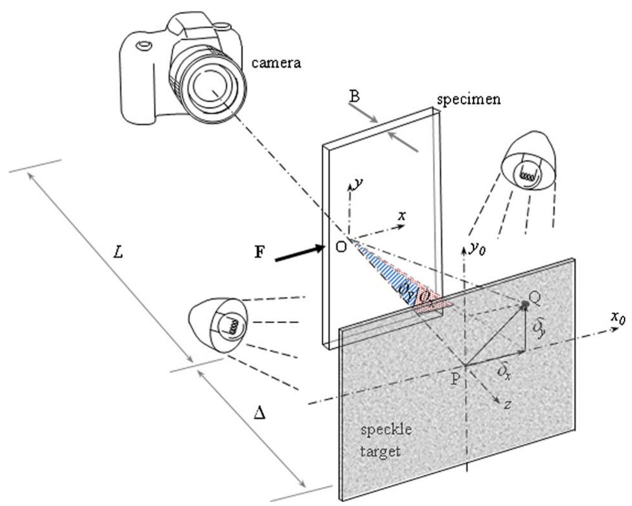

Fig. 1. (Color online) Experimental setup for the DGS method to determine planar stress gradients in phase objects.

3. Working Principle

In Fig. 1, let the in-plane coordinates of the specimen and target planes be denoted (x, y) and (x_0, y_0), respectively, and the optical axis of the setup coincides with the z-axis. Let the speckles on the target plate be photographed normally through the transparent specimen of nominal thickness B and refractive index n in its reference (no-load) state. That is, a generic point P on the target plane, corresponding to point O on the specimen (object) plane, is recorded by the camera in the reference state. When subjected to mechanical load (e.g., due to force F acting on the edge of the specimen in Fig. 1), both refractive index and thickness changes occur throughout the specimen depending on the local state of stress. A combination of these changes causes light rays to deflect. That is, the light ray $\overline{OP}$ in the reference/undeformed state now corresponds to $\overline{OQ}$ after the specimen deforms. By quantifying the spatial vector $\overline{PQ}$ and knowing the separation distance Δ between the mid-plane of the specimen and target, the angular deflection ϕ of the light ray can be determined relative to the optical axis.

Let $\hat{i}, \hat{j}$, and $\hat{k}$ denote unit vectors for the Cartesian coordinates defined with point O as the origin. When the specimen is undeformed, the unit vector $\hat{k}$ is collinear with $\overline{OP}$, bringing point $P(x_0, y_0)$ to focus when imaged by the camera via point $O(x, y)$. Upon deformation, the optical path is locally perturbed, thereby bringing a neighboring point $Q(x_0 = \delta_x, y_0 = \delta_y)$ to focus. Here δ_x and δ_y denote components of the vector $\overline{PQ}$ in the x- and y-directions. Let the unit vector corresponding to the perturbed optical path $\overline{OQ}$ be

$$\hat{d} = \alpha\hat{i} + \beta\hat{j} + \gamma\hat{k}, \tag{1}$$

where α, β, and γ are the direction cosines of $\hat{d}$, and ϕ_x and ϕ_y are angular deflections in the x-z and y-z planes, respectively, as shown in Fig. 2.

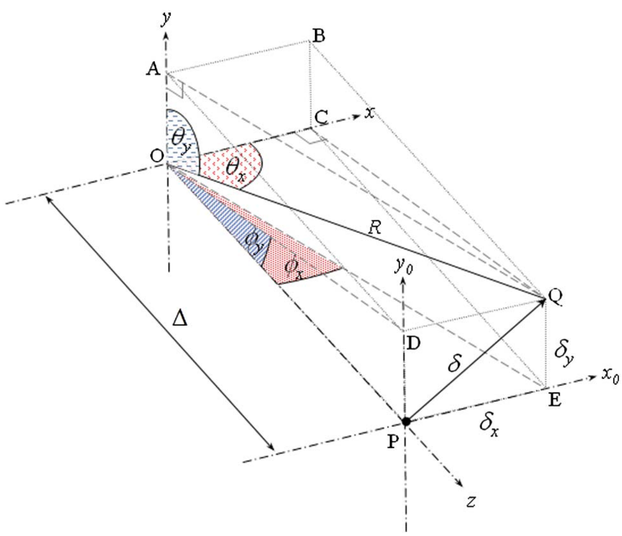

Fig. 2. (Color online) Working principle of DGS.

If the initial thickness and refractive index of the specimen are B and n, respectively, the optical path change, δS, for symmetric deformation of the specimen about the mid-plane in the z-direction, is given by the elasto-optical equation [12]

$$\delta S(x, y) = 2B(n-1)\int_0^{1/2} \varepsilon_{zz} d(z/B) + 2B\int_0^{1/2} \delta n d(z/B). \tag{2}$$

The two terms in the above equation represent the contribution of normal strain in the thickness direction, ε_{zz}, and the change in the refractive index, δn, to the overall optical path change, respectively. The refractive index change caused by local normal stress in the specimen is given by the well-known Maxwell–Neumann relation [19]

$$\delta n(x, y) = D_1(\sigma_{xx} + \sigma_{yy} + \sigma_{zz}), \tag{3}$$

where D_1 is the stress-optic constant of an optically isotropic solid and σ_{xx}, σ_{yy}, and σ_{zz} are normal stresses in the x-, y-, and z-directions, respectively. Using generalized Hooke's law for an isotropic, linear elastic solid, the normal strain component ε_{zz} can be related to normal stresses $(\varepsilon_{zz} = \frac{1}{E}[\sigma_{zz} - \upsilon(\sigma_{xx} + \sigma_{yy})])$. That is, Eq. (2) can be written as

$$\delta S = 2B\left(D_1 - \frac{\upsilon}{E}(n-1)\right) \times \int_0^{1/2}\left\{(\sigma_{xx}+\sigma_{yy})\left[1 + D_2\left(\frac{\sigma_{zz}}{\upsilon(\sigma_{xx}+\sigma_{yy})}\right)\right]\right\} d(z/B), \tag{4}$$

where $D_2 = [\upsilon D_1 + \upsilon(n-1)/E]/[D_1 - \upsilon(n-1)/E]$, E is the Young's modulus, and υ is the Poisson's ratio of the transparent solid. In the above equation, the second term $D_2(\frac{\sigma_{zz}}{\upsilon(\sigma_{xx}+\sigma_{yy})})$ represents the degree of plane strain that can be neglected for applications where plane stress assumptions (in-plane dimensions $\gg$ thickness of the specimen and $\sigma_{zz} \simeq 0$) are reasonable. Thus, for plane stress conditions, Eq. (4) reduces to

$$\delta S(x, y) \approx C_\sigma B(\sigma_{xx} + \sigma_{yy}), \tag{5}$$

where $C_\sigma = D_1 - (\upsilon/E)(n-1)$ is the elasto-optic constant of the specimen material. In Eq. (5), the normal stress components σ_{xx} and σ_{yy} denote *integrated values over the specimen thickness*.

The angular deflection of a generic light ray is caused by the change in the optical path due to elasto-optic effects. Hence, the propagation vector can be related to the optical path change as [12,20]

$$\hat{d} \approx \frac{\partial(\delta S)}{\partial x}\hat{i} + \frac{\partial(\delta S)}{\partial y}\hat{j} + \hat{k} \tag{6}$$

for small spatial gradients. From Eqs. (1), (5), and (6), for small angular deflections, the direction cosines

α and β are proportional to in-plane stress gradients as,

$$\alpha = \frac{\partial(\delta S)}{\partial x} = C_\sigma B \frac{\partial(\sigma_{xx} + \sigma_{yy})}{\partial x} \quad \text{and}$$
$$\beta = \frac{\partial(\delta S)}{\partial y} = C_\sigma B \frac{\partial(\sigma_{xx} + \sigma_{yy})}{\partial y}. \tag{7}$$

A geometric analysis of the perturbed ray $\overline{OQ}$ reveals the relationship between direction cosines α and β and angular deflection components ϕ_x and ϕ_y, respectively. Referring to Fig. 2, the perturbed ray subtends solid angles θ_x and θ_y with the x- and y-axes. The angular deflections ϕ_x and ϕ_y as defined earlier are also shown in Fig. 2. With reference to the planes defined by OQC, OQA, OPE and OPD,

$$\cos\theta_x = \frac{\delta_x}{R}, \qquad \cos\theta_y = \frac{\delta_y}{R},$$
$$\tan\phi_x = \frac{\delta_x}{\Delta}, \quad \text{and} \quad \tan\phi_y = \frac{\delta_y}{\Delta}, \tag{8}$$

where $R(=\sqrt{\Delta^2 + \delta_x^2 + \delta_y^2})$ is the distance between O and Q. From the above, expressions for the angular deflection components can be obtained as

$$\tan\phi_x = \frac{R}{\Delta}\cos\theta_x = \sqrt{1 + \frac{\delta_x^2 + \delta_y^2}{\Delta^2}}\cos\theta_x,$$
$$\tan\phi_y = \frac{R}{\Delta}\cos\theta_y = \sqrt{1 + \frac{\delta_x^2 + \delta_y^2}{\Delta^2}}\cos\theta_y. \tag{9}$$

It can be noted from Eq. (9) that for small angular deflections (or, δ_x, $\delta_y \ll \Delta$), the expressions reduce to $\phi_x \approx \cos\theta_x = \alpha$ and $\phi_y \approx \cos\theta_y = \beta$. Thus, for the case of small angular deflections of light rays, Eq. (7) reduces to

$$\phi_x \approx \alpha = C_\sigma B \frac{\partial(\sigma_{xx} + \sigma_{yy})}{\partial x},$$
$$\phi_y \approx \beta = C_\sigma B \frac{\partial(\sigma_{xx} + \sigma_{yy})}{\partial y}, \tag{10}$$

which serve as the governing equations for the method and can be used to obtain stress gradients when specimen parameters C_σ and B are known.

The above governing equations reveal that the angular deflections ϕ_x and ϕ_y, and hence stress gradients in the x- and y-directions, can be obtained by quantifying local displacements δ_x, δ_y values first and then dividing them by the separation distance Δ. The displacements δ_x, δ_y can be evaluated by carrying out a conventional 2D DIC between speckle images recorded in the reference and deformed states of the specimen. Hence the new method is aptly named DGS. A subtle but important point to note here is that displacements δ_x, δ_y are evaluated on the target plane whose coordinates are (x_0, y_0), but can be replaced with the specimen plane coordinates (x, y) for $\Delta \ll L$(see Fig. 1). Further justification of this assumption is provided later on.

From Eq. (10) it can be noted that the sensitivity of measurement of angular deflections $\phi_x$and ϕ_y is dependent on two parameters δ_x (or δ_y) and Δ, which provides added flexibility. The sensitivity of in-plane displacement measurement (of δ_x or δ_y) is typically dictated by a number of parameters that affect 2D digital image correlation methods, including speckle characteristics/size, pixel size, sensor resolution, and image processing algorithm employed. For the sake of brevity, discussion of those issues is avoided here and can be found elsewhere [3]. For the speckle and camera parameters used in this study, in plane displacement resolution is in the 3–4 μm range as demonstrated in the works of Tippur and his coworkers [21,22].

It is also interesting to note that Eq. (10) shows that DGS method measures quantities identical to the ones measured by the CGS method [10–12,23]. However, *unlike* CGS, DGS can be used to measure two orthogonal stress gradients in transparent solids *simultaneously* and does not use any coherent optics. This capability can be exploited for determining stresses $(\sigma_{xx} + \sigma_{yy})$ from measured stress gradients, as shown later in Section 6.

4. Calibration Experiment

To verify the DGS method, first the problem with a well-defined angular deflection field of light rays produced by a plano-convex lens was studied. A target plane with the speckle pattern was placed at a sufficiently large distance ($L \approx 1000$ mm) from a recording camera (Nikon D100 digital camera fitted with a 28–300 mm lens using an extension tube and aperture setting #11). A reference (undeformed) image of the speckle pattern was recorded first. Then, a *thin* plano-convex lens of a relatively long effective focal length, $f_l = 1000$ mm and clear aperture of 80 mm diameter was introduced between the camera and the speckle plane. The choice of a long focal length thin lens allowed for relatively small angular deflections of light rays. The distance Δ from the effective center of the lens to the speckle plane was 19.4 mm. Care was exercised to align the center of the plano-convex lens close to the optical axis of the camera. A second image of the speckle pattern, this time through the plano-convex lens, was recorded. The size of the image recorded by the camera was approximately 60 mm × 40 mm rectangle in the central region of the plano-convex lens. The recording of the reference and perturbed speckle fields used a pixel resolution of 1504 × 1000 pixels (1 pixel = 39.5 μm on the target plane). The second speckle image can be considered to be the "deformed" or "perturbed" image whose angular deflection fields are given by

$$\phi_x = \frac{\partial}{\partial x}\left(\frac{x^2+y^2}{2f_l}\right) = \frac{x}{f_l} \quad \text{and}$$
$$\phi_y = \frac{\partial}{\partial y}\left(\frac{x^2+y^2}{2f_l}\right) = \frac{y}{f_l}, \tag{11}$$

where $(\frac{x^2+y^2}{2f_l})$ describes the spherical wavefront due to the plano-convex lens, and ϕ_x and ϕ_y are the angular deflection fields with respect to the unperturbed speckle image. As evident from the above equations, the two orthogonal angular deflection fields are linear functions of the lens plane coordinates, x and y. Hence, the contours of constant ϕ_x and ϕ_y should be equally spaced with their principal directions in the x- and y-directions, respectively.

To obtain the ϕ_x and ϕ_y fields, the in-plane displacement fields (δ_x and δ_y) were first extracted from images by performing 2D digital image correlation between the reference and perturbed speckle recordings using a commercial DIC software, ARAMIS. During the analysis, the images were segmented into 64×91 nonoverlapping facets or sub-images resulting in an array of 64×91 data points. For small in-plane displacements (δ_x and $\delta_y \ll \Delta$), angular deflection fields were obtained, such as $\phi_x \approx \frac{\delta_x}{\Delta}$ and $\phi_y \approx \frac{\delta_y}{\Delta}$. (The maximum values of δ_x and δ_y were less than 300 μm.) The contour plots of the experimentally obtained ϕ_x, ϕ_y, and the resultant angle $\phi(= \sqrt{\phi_x^2 + \phi_y^2})$ fields are shown in Fig. 3. As predicted, the contours of ϕ_x and ϕ_y are equidistant parallel lines along the x- and y-directions, respectively, and the contours of ϕ are equally spaced concentric circles centered on the optical axis of the lens.

If the angular deflection fields are known, it is also possible to quantify the focal length of the plano-convex lens using Eq. (11) as, $f_l = \frac{x}{\phi_x} = \frac{y}{\phi_y}$. For this experiment, the measured focal lengths were 973 ± 32 mm from the ϕ_x field and 988 ± 42 mm from the ϕ_y field. These are within 3% of the manufacturer-provided focal length of 1000 mm for the lens.

As noted in the previous section, in the DGS technique, the camera is focused on the target plane through the phase object. Yet, the analysis uses the coordinates of the specimen's (phase object) mid-plane situated at a distance of Δ away from the target interchangeably. This introduces a perspective (or gap) effect. That is, a point $O(x, y)$ on the specimen corresponds to a point $P(x_0, y_0)$ on the target plane as shown in the 2D schematic (see Fig. 4). This can be taken into account by a mapping function between the specimen and the target planes. With reference to Fig. 4, $\tan\theta = \frac{y_s}{L} = \frac{y_t}{L+\Delta}$, where y_s and y_t are coordinates of the specimen and target planes. This can be used to account for the coordinates of the specimen plane as $y_s = (\frac{L}{L+\Delta})y_t$. A similar mapping function for the horizontal coordinate is obvious and implied. Using these relations, the contours of ϕ_x and ϕ_y for the plano-convex lens were obtained and are shown (broken lines) in Fig. 5 along with the contours without any correction (solid lines). Evidently, for the chosen experimental parameters, the differences are rather negligible in the entire field. The errors close to the optical axis are minimum whereas they increase as one moves away from the optical axis.

5. Line Load on the Edge of a Planar Sheet

Next, a stress concentration problem of a line load acting on the edge of a large planar sheet was studied using the DGS method. A large (180 mm × 69.5 mm) rectangular sheet of clear PMMA specimen (Young's modulus = 3300 MPa, Poisson's ratio = 0.35, and $C_\sigma \sim -1 \times 10^{-10}$ m^2/N) of thickness (B) 9.4 mm was used in the experiment. The actual experimental setup is shown in Fig. 6. The specimen was placed on a flat rigid base and subjected to line loading using a cylindrical steel pin (7.7 mm diam.). A 5 kN capacity Instron 4465 universal testing machine was used in displacement controlled mode (cross-head speed 0.005 mm/ sec) to load the specimen. A target plate painted with random black and white speckles was placed at a distance $\Delta(= 30$ mm) away from the specimen using an experimental setup similar to the one shown in Fig. 1. Multiple heavy black dots of known spacing between them were marked on the speckle plane to relate the image dimensions to the actual specimen/target dimensions. A Nikon D100 digital SLR camera with a 28–300 mm focal length lens (aperture setting #11) and an extension tube were

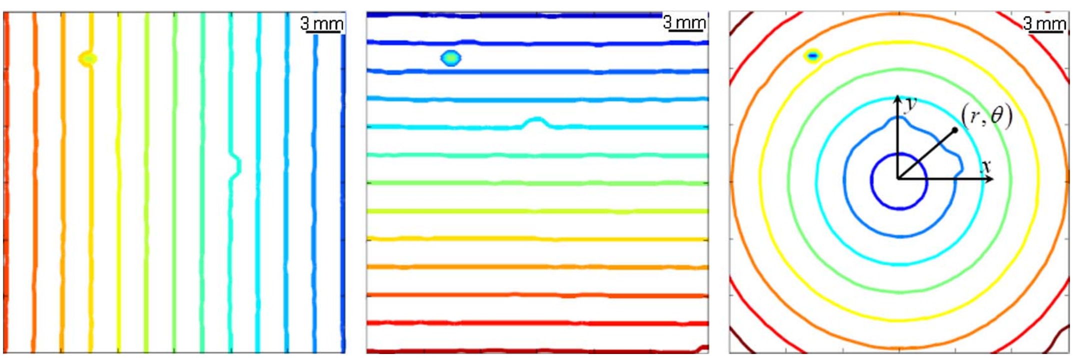

Fig. 3. (Color online) Contour plots of angular deflections (left to right) ϕ_x, ϕ_y and ϕ fields caused by a plano-convex spherical lens. Contour interval = 2.5×10^{-3} rads. (The heavy dot in the angular deflection field is due to a reference mark on the speckle plate.)

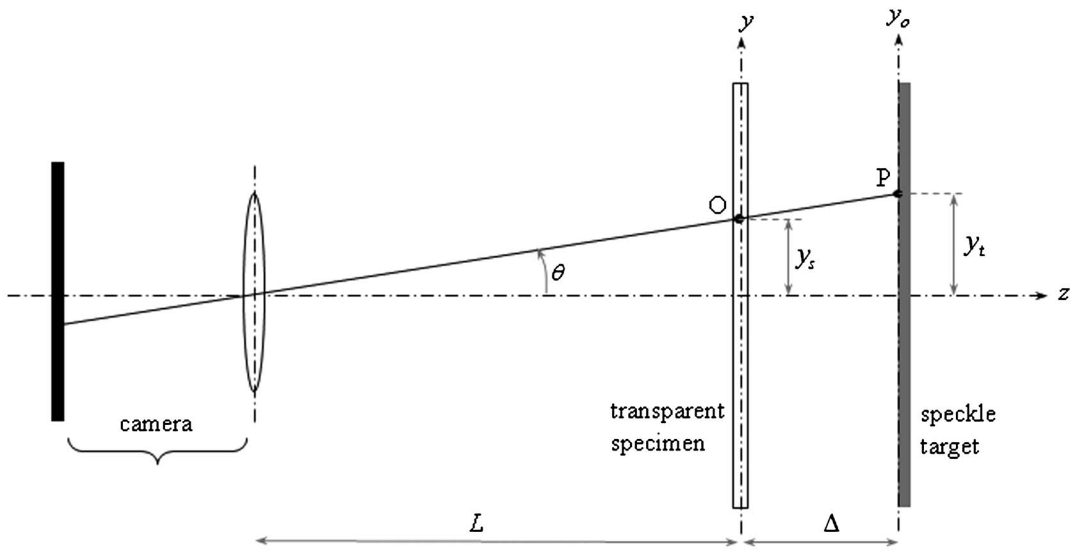

Fig. 4. Mapping coordinates of specimen and target planes.

used to record speckles through the specimen in the load vicinity. The camera was situated at a distance L of approximately 1040 mm from the specimen.

At a small load (of a few Newtons), a reference image of the target was recorded through the transparent specimen. As the load was increased gradually, speckle images were recorded using time-lapse photography (one frame every five seconds once) at different load levels. One of the speckle images in the load point vicinity corresponding to a 3520 N load is shown in Fig. 7. A careful examination of the image shows noticeable distortion/blurring of speckles near the loading point, whereas they appear relatively unaffected at far-away locations. The digitized speckle images (1504×1000 pixels) recorded at different load levels were correlated with the one corresponding to no-load/reference condition using a 2D digital image correlation software, ARAMIS. As described previously, an array of in-plane speckle displacements on the target plane (and hence the specimen plane) was evaluated and converted into local angular deflections of light rays ϕ_x and ϕ_y. A facet/sub-image size of 15×15 pixels (1 pixel = 36.5 μm on the target plane) without any overlap was used in the image correlation analysis for extracting displacement components. Figure 8 shows the resulting contours of ϕ_x and ϕ_y for three representative load levels in a square region around the loading point. *It is important to note that it is essential to account for rigid body motions and impose proper boundary conditions of the problem to quantify the contour levels for further analysis*. That is, in the current problem, the boundary conditions, such as asymmetric stress gradients (ϕ_y) in the y direction about the x axis, symmetric stress gradients (ϕ_x) in the x direction about the x axis, vanishing stress gradients far away from the loading point, and stress-free surfaces along the loading edge of the specimen can all be utilized.

It is well known that the plane stress field near the line load acting on an elastic half-space is given by the Flamant solution as [24]

$$\sigma_{xx} + \sigma_{yy} = \sigma_{rr} = -\frac{2F}{\pi B}\frac{\cos(\theta)}{r} = -\frac{2F}{\pi B}\frac{x}{r^2},$$
$$\sigma_{\theta\theta} = 0, \qquad \sigma_{r\theta} = 0, \tag{12}$$

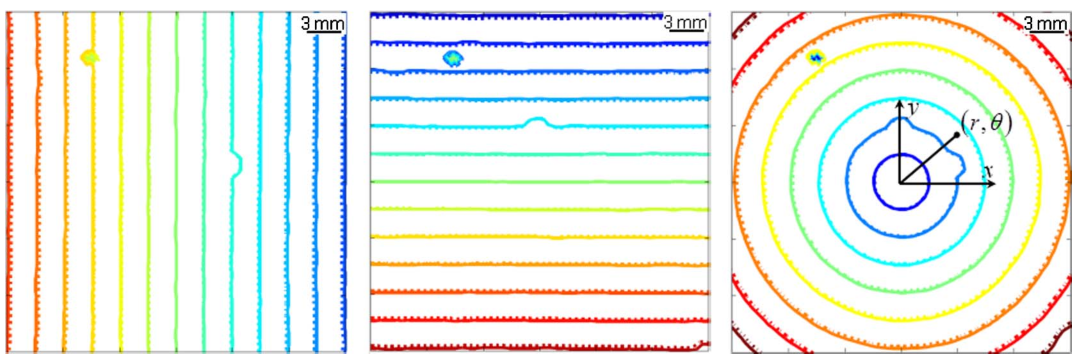

Fig. 5. (Color online) Contour plots of angular deflections of corrected (broken lines) and uncorrected (solid lines) for (left) ϕ_x, (middle) ϕ_y, and (right) ϕ fields caused by a long focal length plano-convex lens. Contour interval = 2.5×10^{-3} rads.

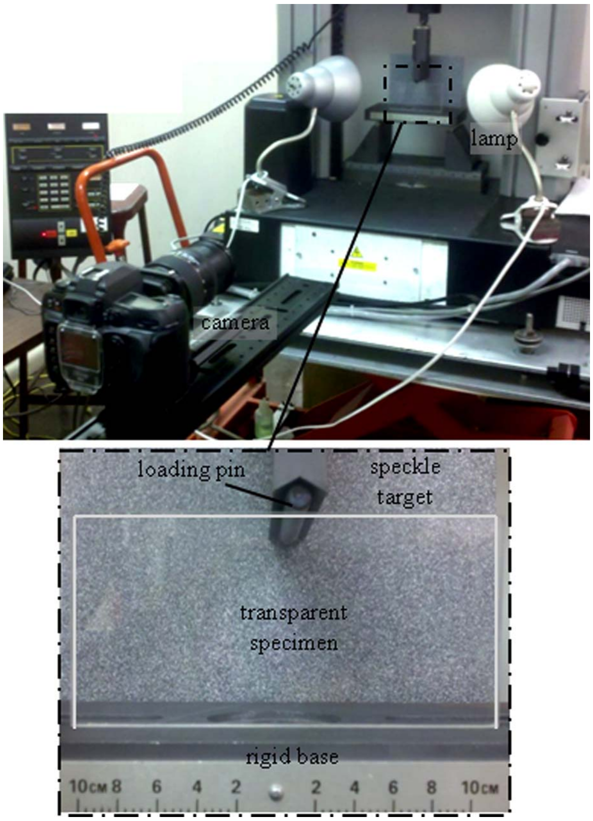

Fig. 6. (Color online) (top) Experimental setup used for studying stress concentration caused by a line load acting on the edge of a large PMMA sheet. (bottom) The close-up shows loading pin resting on the top edge of the transparent specimen and speckles on the target.

where F is the applied load, B is the thickness of the half-space and (r, θ) and (x, y) are the polar and Cartesian coordinates, respectively, as shown in Fig. 7. Note that the hoop stress $\sigma_{\theta\theta}$ and shear stress $\sigma_{r\theta}$ vanish for the Flamant solution. Since $(\sigma_{xx} + \sigma_{yy}) =$

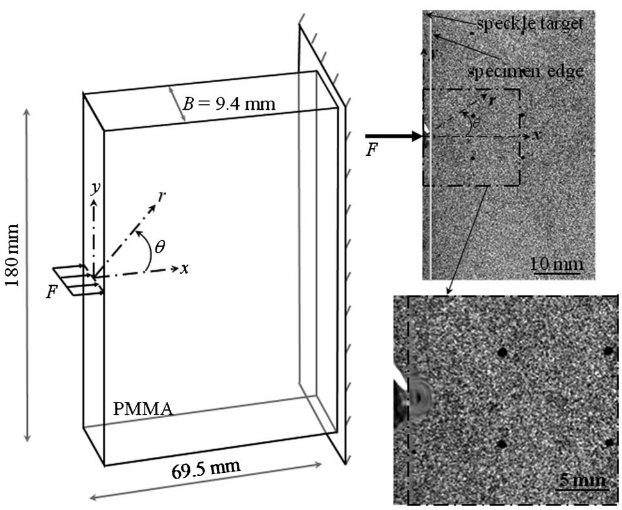

Fig. 7. Line load acting on a (left) half-space and (right) an actual speckle image recorded. Note the blurred/distorted region adjacent to the loading pin in the enlarged speckle image.

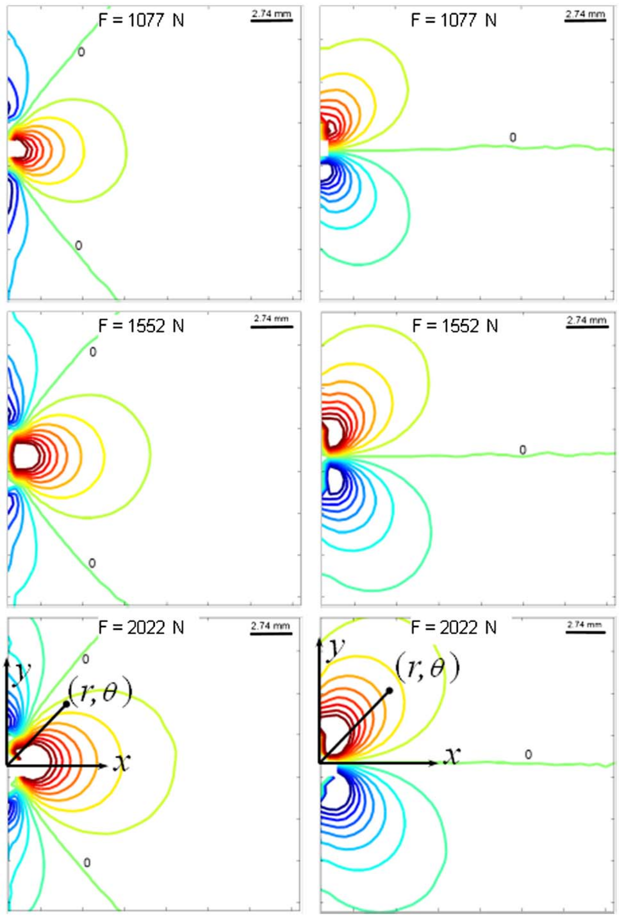

Fig. 8. (Color online) Measured (left) ϕ_x and (right) ϕ_y contours near the loading point for different load levels. Contour interval $= 1 \times 10^{-3}$ rads. (The left vertical edge of each image corresponds to the loading edge where F acts at the origin.)

$(\sigma_{rr} + \sigma_{\theta\theta})$ in plane stress, the normal (nonzero) radial stress σ_{rr} becomes singular/unbounded as the loading point $(r \to 0)$ is approached. Therefore, the in-plane stress invariant in a half-space subjected to line load equals the normal stress in the radial direction. From Eqs. (10) and (12),

$$\phi_x = C_\sigma B \frac{\partial(\sigma_{xx} + \sigma_{yy})}{\partial x} = C_\sigma B \frac{\partial(\sigma_{rr})}{\partial x} \quad \text{and}$$
$$\phi_y = C_\sigma B \frac{\partial(\sigma_{xx} + \sigma_{yy})}{\partial y} = C_\sigma B \frac{\partial(\sigma_{rr})}{\partial y}. \tag{13}$$

Using Eqs. (12) and (13), the equations for the ϕ_x and ϕ_y fields can be expressed as

$$\phi_x = C_\sigma B \frac{2F}{\pi B} \frac{\cos(2\theta)}{r^2} \quad \text{and} \quad \phi_y = C_\sigma B \frac{2F}{\pi B} \frac{\sin(2\theta)}{r^2}. \tag{14}$$

For comparison, the experimental and analytical angular deflection contours for the case of $F =$ 2022 N are shown in Fig. 9. The dominant triaxial stress region where plane stress assumptions are violated are expected close to the loading point. In

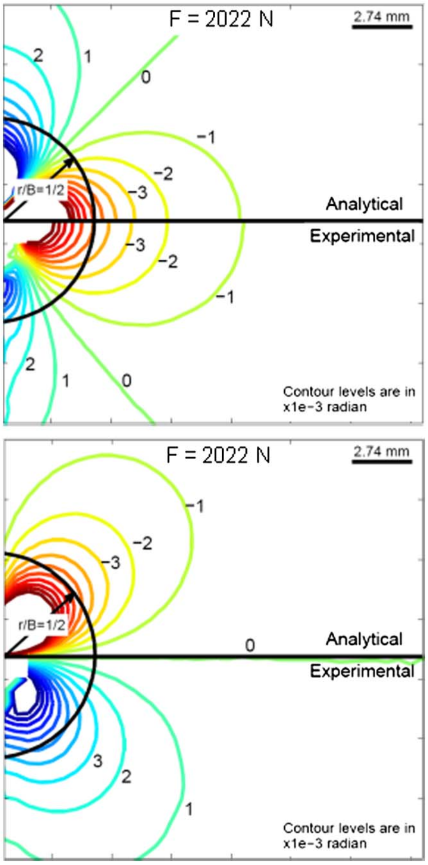

Fig. 9. (Color online) Comparison of experimental and analytical (top) ϕ_x and (bottom) ϕ_y contours for $F = 2022$ N.

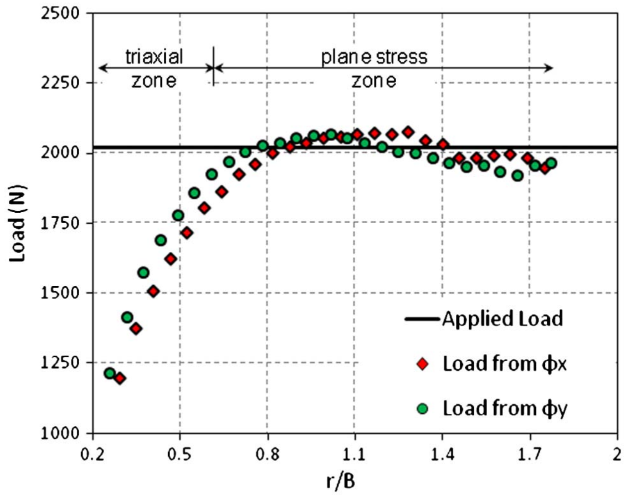

Fig. 10. (Color online) Plot of experimentally extracted load (symbols) at various radial locations from the two angular deflection fields ϕ_x and ϕ_y along r, $\theta = 0°$ and r, $\theta = 45°$, respectively. Deviation between the Flamant solution and measurement close to the loading point where plane stress approximations are violated can be seen.

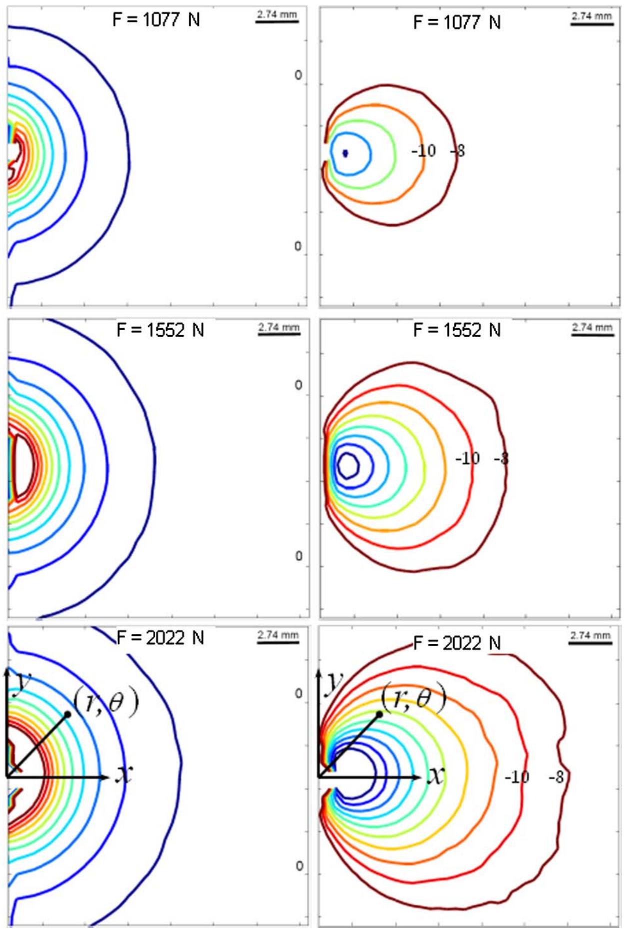

Fig. 11. (Color online) Measured resultant angular deflection of light rays (left column) $\phi$and (right column) estimated radial stress σ_{rr} contours for various load levels. Contours are plotted every 1×10^{-3} rads and 2 MPa, respectively. (The left vertical edge in each image is the edge where the line load acts horizontally at the origin.)

cracked bodies where a stress singularity of $r^{-1/2}$ prevails, a zone of dominant stress triaxiality has been shown to exist near the crack tip ($0 \leq r/B \leq 1/2$) [12]. Based on that observation and assuming a dominant triaxial stress region of similar size to occur in the current case as well, agreement between analytical solutions and experiment measurements are not expected to be good at least up to $r/B = 1/2$, shown in Fig. 9 as a semi-circle centered around the origin. In the regions outside the zone of dominant triaxiality, a good qualitative and quantitative agreement between experimental and analytical contours can be seen.

The ϕ_x and ϕ_y data corresponding to a particular load case were used to back calculate the load F from Eq. (14). Figure 10 shows the plot of load as a function of r/B along $\theta = 0°$ and $\theta = 45°$ calculated from ϕ_x and ϕ_y fields, respectively, for the case when $F = 2022$ N. From the graph, it can be seen that, after an initial nonconformity up to $r/B \sim 0.6$ in the dominant triaxiality region, the extracted load (symbols) values agree with the applied load measured from the testing machine (solid curve), further confirming the previous observations.

6. Estimation of Stresses From Stress Gradients

Since DGS is capable of measuring stress gradients in two orthogonal directions simultaneously, one can estimate the stresses $(\sigma_{xx} + \sigma_{yy})(= \sigma_{rr}$ in this case), in the region of interest from measured gradients. This can be done as follows:

Using Eq. (14), the resultant of ϕ_x and ϕ_y can be obtained as

$$\phi = \sqrt{\phi_x^2 + \phi_y^2} = C_\sigma B \frac{2F}{\pi B r^2}. \tag{15}$$

Evidently, the expression for ϕ in Eq. (15) is independent of θ, suggesting that contours of ϕ are circular (semi-circular in this case) relative to the origin. This can be verified by generating contours of ϕ from measured ϕ_x and ϕ_y, that is, for each facet/sub-image, ϕ value was computed in the load point vicinity. The first column in Fig. 11 shows the measured contours of ϕ for the three load levels considered in Fig. 8. The resulting contours are indeed semi-circular (except near the free edge of the specimen where edge effects affect ϕ_x and ϕ_y computations) centered about the loading point, confirming the prediction by the Flamant solution. A direct comparison of measured ϕ values with the predicted ones from Flamant solution is presented in Fig. 12 (top) for a representative case showing a good agreement between the two.

Now, by inspecting the analytical expressions of ϕ [Eq. (15) and Eq. (12)], it becomes clear that stress $\sigma_{rr}(= \sigma_{xx} + \sigma_{yy})$ can be estimated under plane stress conditions by simply multiplying ϕ values with the corresponding $(r \cos \theta)$values if ϕ data are available from experimental measurements as $(\sigma_{xx} + \sigma_{yy}) = \sigma_{rr} = \frac{\phi}{C_\sigma B}(r \cos \theta)$.The second column in Fig. 11 shows the stress contours thus obtained for all the three load levels considered in Fig. 8. The contour plots of the experimentally estimated and analytical stress fields for a representative case of $F = 2022$ N are shown in Fig. 12. Again a good agreement between estimated and predicted contours of normal stress σ_{rr} near the loading point where plane stress conditions exist is seen demonstrating the viability of the DGS method for stress estimation purposes besides stress gradient measurement in this case.

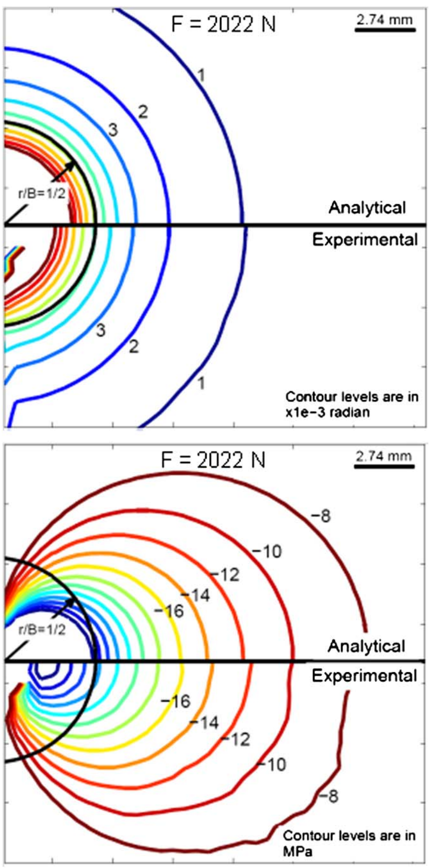

Fig. 12. (Color online) Comparison between experimental and analytical (top) ϕ and (bottom) radial stress (σ_{rr}) contours for $F = 2022$ N.

It should be emphasized here that direct numerical integration of measured stress gradients could also be used to estimate $\sigma_{rr}(= \sigma_{xx} + \sigma_{yy})$ if far-field boundary conditions are known.

7. Conclusions

An optical method, digital gradient sensing (DGS), based on elasto-optic effect and digital image correlation methodology is proposed for measuring stress gradients in transparent planar objects. The method employs a relatively simple experimental setup and does not use coherent optics. The reliance of the method on prevailing digital recording technology and image processing algorithms used for digital image correlation/registration methods offers additional advantages. The potential of the method to inspect and evaluate phase objects (such as lenses) or characterize the mechanical performance of transparent structural materials (such as transparent armor) subjected to external loads is enormous.

Here, the working principle of DGS has been explained, and the necessary governing equations have been derived. The analysis shows that the method is capable of measuring small angular deflections of light rays produced by *nonuniform* changes in the thickness and/or refractive index of the material. In mechanically loaded planar objects, the angular deflections are in turn related to the gradients of the first invariant of stresses, namely $\frac{\partial(\sigma_{xx}+\sigma_{yy})}{\partial x}$ or $\frac{\partial(\sigma_{xx}+\sigma_{yy})}{\partial y}$ under plane stress conditions. The possibility of measuring such stress gradients in two orthogonal directions, *simultaneously*, makes it possible to estimate stresses $(\sigma_{xx} + \sigma_{yy})$when aided by analytical expressions.

The DGS method has been first demonstrated using angular deflection fields produced by a plano-convex spherical lens. The measured contours of constant angular deflection of light rays and the deduced focal length are in good agreement with the expected value. The method has also been successfully implemented to study a stress concentration problem involving a line load acting on the edge of a large planar sheet. Again, the measured stress gradients parallel and perpendicular to the loading direction have been measured and are in good agreement with the predictions based on an idealized Flamant solution in regions where plane stress conditions hold. Aided by the functional form of the Flamant solution, the two orthogonal stress gradients have also been combined to estimate the radial stresses in the load point vicinity.

Partial support for this work through grant W911NF-08-1-0285 from the U.S. Army Research Office is gratefully acknowledged.

References

1. W. N. Sharpe, ed., *Handbook of Experimental Solid Mechanics* (Springer, 2008).
2. N. Shukla and J. W. Dally, *Experimental Solid Mechanics* (College House, 2010).
3. M. A. Sutton, U. Orteu, and H. Schreier, *Image Correlation for Shape, Motion and Deformation Measurements* (Springer, 2009).
4. E. Strassburger, "Ballistic testing of transparent armour ceramics," J. Eur. Ceram. Soc. **29**, 267–273 (2009).
5. P. Patel, G. A. Gilde, P. G. Dehmer, and J. W. McCauley, "Transparent armor," AMPTIAC Newsletter **4**(3), 1–9 (2000).
6. S. Iwamoto, A. N. Nakagaito, H. Yano, and M. Nogi, "Optically transparent composites reinforced with plant fiber-based nanofibers," Appl. Phys. A: Mater. Sci. Process. **81**, 1109–1112 (2005).
7. E. J. A. Pope, M. Asami, and J. D. Mackenzie, "Transparent silica gel-PMMA composites," J. Mater. Res. **4**, 1018–1026 (1989).
8. S. Ravi, "Development of transparent composite for photoelastic studies," Adv. Compos. Mater. **7**, 73–81 (1998).
9. H. Yano, J. Sugiyama, A. N. Nakagaito, M. Nogi, T. Matsuura, M. Hikita, and K. Handa, "Optically transparent composites reinforced with networks of bacterial nanofibers," Adv. Mater. **17**, 153–155 (2005).
10. H. V. Tippur, "Coherent gradient sensing—a Fourier optics analysis and applications to fracture," Appl. Opt. **31**, 4428–4439 (1992).
11. H. V. Tippur, "Coherent gradient sensing (CGS) method for fracture mechanics: a review," Fatigue Fract. Eng. Mater. Struct. **33**, 832–858 (2010).
12. H. V. Tippur, S. Krishnaswamy, and A. J. Rosakis, "Optical mapping of crack tip deformations using the methods of transmission and reflection coherent gradient sensing—a study of crack tip K-dominance," Int. J. Fract. **52**, 91–117 (1991).
13. H. V. Tippur and A. J. Rosakis, "Quasi-static and dynamic crack-growth along bimaterial interfaces—a note on crack-tip field-measurements using coherent gradient sensing," Exp. Mech. **31**, 243–251 (1991).
14. J. Kimberley and J. Lambros, "Dynamic crack kinking from a PMMA/homalite interface," Exp. Mech. **44**, 158–166 (2004).
15. J. J. Mason, J. Lambros, and A. J. Rosakis, "The use of a coherent gradient sensor in dynamic mixed-mode fracture-mechanics experiments," J. Mech. Phys. Solids **40**, 641–661 (1992).
16. S. Ramaswamy, H. V. Tippur, and L. Xu, "Mixed-mode crack-tip deformations studied using a modified flexural specimen and coherent gradient sensing," Exp. Mech. **33**, 218–227 (1993).
17. J. K. Sinha, H. V. Tippur, and L. M. Xu, "An interferometric and finite element investigation of interfacial crack tip fields: role of mode-mixity on 3-D stress variations," Int. J. Solids Struct. **34**, 741–754 (1997).
18. X. J. Dai, H. Yun, and Q. Pu, "Measuring thickness change of transparent plate by electronic speckle pattern interferometry and digital image correlation," Opt. Commun. **283**, 3481–3486 (2010).
19. J. W. Dally and W. F. Riley, *Experimental Stress Analysis*, 4th ed. (College House, 2005).
20. M. Born and E. Wolf, *Principles of Optics*, 7th ed. (Cambridge, 1999).
21. M. S. Kirugulige, H. V. Tippur, and T. S. Denney, "Measurement of transient deformations using digital image correlation method and high-speed photography: application to dynamic fracture," Appl. Opt. **46**, 5083–5096 (2007).
22. M. S. Kirugulige and H. V. Tippur, "Measurement of surface deformations and fracture parameters for a mixed-mode crack driven by stress waves using image correlation technique and high-speed photography," Strain **45**, 108–122 (2009).
23. H. V. Tippur, S. Krishnaswamy, and A. J. Rosakis, "A coherent gradient sensor for crack tip deformation measurements—analysis and experimental results," Int. J. Fract. **48**, 193–204 (1991).
24. R. G. Budynas, *Advanced Strength and Applied Stress Analysis* (McGraw-Hill, 1998).